Scanning microelectrochemical characterization of the effect of polarization on the localized corrosion of 304 stainless steel in chloride solution

J. Izquierdo[1,2], L. Martín-Ruíz[1], B.M. Fernández-Pérez[1], R. Rodríguez-Raposo[1], J.J. Santana[3], R.M. Souto[1,2]

[1] *Department of Chemistry, University of La Laguna, E-38071 La Laguna (Tenerife), Spain.*

[2] *Instituto Universitario de Materiales y Nanotecnologías, University of La Laguna, E-38200 La Laguna (Tenerife), Spain.*

[3] *Department of Process Engineering, University of Las Palmas de Gran Canaria, E-35017 Las Palmas de Gran Canaria, Spain.*

Abstract

Corrosion processes occurring on stainless steel 304 surfaces under anodic polarization have been characterized using scanning electrochemical microscopy (SECM) and the scanning vibrating electrode technique (SVET), complemented with conventional potentiodynamic polarization curves. Stable pit formation has been detected by SVET on the samples as result of surface modification under electrochemical control, which may include the previous electrochemical reduction of passive oxide layer if the media is not aggressive enough to induce pitting at small overpotentials. Additionally, the sample generation – tip collection operation mode of the SECM has enabled the detection of local release of iron (II) ions, as well as their conversion to iron (III), both processes being greatly affected by the potential applied to the substrate.

Keywords: 304 stainless steel; Pitting corrosion; Polarization; Scanning electrochemical microscopy; Scanning vibrating electrode technique; Chloride ions.

1. Introduction

Corrosion problems affecting metals have been recognized for centuries, especially in relation to iron and iron-based materials, the most widely employed metallic materials in human societies. Yet, due to their mechanical and electrical properties, iron and steel structures have shown to be valuable enough to still being extensively applied for many industrial purposes. Their degradation accounts for a major portion of the total cost of corrosion in most industrialized countries, which supposes annual economic losses up to 5 % of the Gross Domestic Product [1]. In order to increase the profitability of these materials, different stainless steels are produced by alloying iron with nobler metals, resulting in enhanced anticorrosion protection [2-7]. Nevertheless, some environments are still able to induce local damage to the protective passive layer, especially when halide ions are present. This kind of attack leads to pitting corrosion, highly localized in character though apparently distributed in random manner. This localized attack is known to have its origins in the formation of microcells, microanodes and microcathodes, distributed along the metal surface despite its apparent homogeneity, arising from small chemical asymmetries in the system. The impact of the early stages of this localized attack are evidenced with the help of topographic imaging techniques like scanning electron microscopy (SEM), which provides support for the intrinsically stochastic distribution of the attack, and assists characterization of the subsequent morphology of the attack [7-15]. *Post-mortem* microscopical observations are also frequently used to establish that the degradation starts within the range of micrometers or below, so that any global measurement performed on the specimen can be interpreted in terms of highly localized processes. However, this interpretation is an assumption based on extrapolations, and both local effects and their mechanisms are not completely understood due to the lack of spatial resolution of conventional techniques.

Due to the electrochemical nature of the corrosion reactions, electrochemical techniques including DC potentiometric polarization curves [16], potentiostatic noise measurements [17], and AC electrochemical techniques [18], have constituted the main sources of information for the analysis of the general behaviour of a corroding system, though unable to supply relevant data to support conclusions at the local scale. In order to understand the mechanisms involving the generation and eventual deactivation of microanodes and microchathodes, real time electrochemical information in the micrometer scale must be collected. Spatially-resolved chemical information is achieved

when electrochemical measurements are performed using capillary microcells [19-21], by selecting small portions of the surface that can be distinguished by some microstructural difference. Yet limitations occur during the characterization of the interactions among distributed heterogeneities present in the surfaces, because the complete surface of the sample is not in contact with the test solution when these local techniques are applied. Conversely, high spatial characterization is achieved using *in situ* AFM. This technique allows monitoring topographical changes occurring on representative areas of the metal when immersed in a liquid phase, though it lacks chemical selectivity [22-24].

These limitations have been the motivation for the development of various microelectrochemical techniques, capable to locally evaluate the corrosion behaviour of the substrate under study by recording electrical and chemical information. Among them, scanning electrochemical microscopy (SECM) provides adequate sensitivity to investigate the interactions of surface features with the electrolytic environment in contact with the surface [25,26]. By adequate selection of the operation mode of SECM, the chemical species participating in corrosion processes can be monitored with high spatial resolution, including chloride anions [27], and changes in proton activity [27-30], as well as other ions and neutral species either produced or consumed in the anodic [31-39] and the cathodic half-cell reactions [30,31,33,35,37,38,40-42]. In addition, the scanning vibrating electrode technique (SVET) has also been widely employed in corrosion studies of iron-based materials, because it images the ionic fluxes of species involved in the electrochemical processes occurring on the corroding surfaces [30,43-54].

The analysis of the chemical nature of the electrochemically active species involved in the corrosion processes can be performed in micrometer dimensions using the SECM. A typical microdisk microelectrode, with dimensions between 10 to 25 μm diameter, can be placed in close proximity to the sample, and be used to scan the surface and collect species either produced or consumed by the substrate undergoing corrosion. Iron (II) can be detected in this way, because it is easily oxidized to iron (III) at the microelectrodes. This reaction has been selected to image metastable pitting, localized corrosion, and protection breakdown on iron-based materials under different environmental conditions [31-39]. On the other hand, the Fe^{2+}/Fe^{3+} couple undergoes a reversible redox reaction in acidic conditions, thus allowing iron (III) species to be imaged over reacting samples as well, from their reduction into ferrous species. Surprisingly, this option has not been exploited in corrosion studies with the SECM until now, probably because iron (II) is regarded to be the main dissolution species and it is produced in significant amount to be effectively detected

in most investigations concerning iron-based materials, and because of the high tendency of ferric ions to precipitate as iron (III) hydroxide.

Information provided by SECM can be complemented with that supplied by SVET, which informs about of the location of the electrochemical reactions that occur over an area provided ion fluxes can be produced in the adjacent electrolytic phase. Thus, ionic fluxes related to anodic and cathodic activity on the surface can be distinguished. Despite the rather wide employment of the technique among corrosion researchers, polarization of the investigated surface was scarcely attempted [43,50,51], and it has been mainly constrained to the coupling of dissimilar metals (i.e., formation of galvanic pairs). This situation may arise from the loss of sensitivity experienced when non perfectly symmetrical ionic fluxes from current sources are produced under polarization conditions from the sample due to the geometry of the counter electrode. This problem remains even if perfectly symmetrical counter electrodes were employed while scanning heterogeneous specimens such as those undergoing corrosion. However, valuable semi-quantitative information on the corrosion processes can still be obtained, as it is shown in this work. In this way, passivity breakdown of the passive layer, and stable pitting corrosion growth were investigated at the same time by considering the average current transients as well as the local ionic currents related to these processes.

The aim of this work is to report a combined electrochemical and microelectrochemical characterization of the passivity breakdown of 304 stainless steel in acidic chlorinated solution on polarized samples. Average electrochemical behaviour has been explored using conventional techniques, whereas spatially resolved distributions of the local ionic fluxes related to anodic and cathodic activities, as well as detection of soluble iron species evolving from the corroding metal substrate, were monitored using SECM and SVET.

2. Experimental

Experiments were performed on 304 grade austenitic stainless steel supplied as sheet of thickness 1 mm by Goodfellow Materials Ltd (Cambridge, UK). The metal was not analysed, but had the specified nominal composition of 17–20% Cr, 8–11% Ni, <2% Mn, <0.08% C, Fe in balance. The steel sheet was cut into strips of 2 cm length and 2 mm width, and next mounted vertically in Epofix (Struers, Ballerup, Denmark) resin sleeves of 3 cm

approximate diameter. In this way, only a 2 mm x 1 mm surface of the material was exposed to the test electrolytes. The mounts were abraded using SiC paper of 1200 and 4000 grit, and subsequently polished using alumina suspension of 0.3 µm particle size. The samples were degreased with ethyl alcohol, cleaned in high purity deionized water, and finally dried under air stream.

The tests were conducted in three chloride containing electrolytes of different compositions, namely 0.1 M NaCl, 0.1 M HCl, and 0.025 M HCl + 0.075 M $HClO_4$. All the reagents were of analytical grade, and solutions were prepared by using ultra pure water purified with a Milli-Q system from Millipore. Measurements were conducted at room temperature (nominally 20 ºC) in the naturally aerated solutions.

Electrochemical tests were performed using an Autolab (Metrohm, Herisau, Switzerland) potentiostat controlled by personal computer. A 3-electrode configuration was used, where the steel sample was the working electrode, completed with an Ag/AgCl/KCl (3M) reference electrode, and a platinum counter electrode. Potentiodynamic polarization measurements were conducted at 1 mV s^{-1} scan rate. The freshly polished surface was left unpolarized for 1 hour in the corresponding test solution to allow a stable reading of the open circuit potential (OCP) to be attained. Then, the cathodic Tafel branch was first separately acquired by polarizing the specimen from the spontaneous corrosion potential down to -0.25 V from the OCP. The sample was then retrieved from the solution and subject to surface grinding and polishing steps as before. After stabilization for 1 hour in the solution, the sample was now polarized in the anodic direction up to +1.20 V vs. Ag/AgCl/KCl (3M), and subsequently potential scan was reversed to monitor the corresponding repassivation behaviour. Measurements were repeated by quadruplicate, and average data were obtained for the characteristic electrochemical parameters.

Scanning electrochemical microscopy (SECM) measurements were carried out with an instrument developed by Sensolytics GmbH (Bochum, Germany). The instrument was built around the same Autolab instrument used for conventional electrochemical measurements, though this time operating also as bipotentiostat in some selected experiments. The electrochemical activity of the metallic substrate was monitored by SECM employing a 10 µm diameter platinum microdisk as the sensing tip. The tip to substrate distance was determined from the measurement of *z*-approach curves above the surrounding resin using the reduction of the molecular oxygen dissolved in the electrolyte. In this case, the SECM was operated in the negative feedback mode, with the tip potential

set at -0.65 V vs. Ag/AgCl/KCl (3M). Once the surface was located, the tip was withdrawn to a distance of 10 µm from the sample surface, and scanned parallel to the surface at a scan rate of to 25 µm s^{-1} to record SECM images. The SECM was operated in the Substrate Generation – Tip Collection mode for the detection of either iron (II) or iron (III) ions evolving from the corroding 304 stainless steel surfaces. These species could be selectively monitored by adequately setting the potential of the Pt microelectrode. The potential of the tip was alternately set at +0.50 and at +0.10 V vs. Ag/AgCl/KCl (3M) to detect the generation of Fe(II) and Fe(III) soluble species, respectively. The Fe(II) species were identified through their oxidation to Fe(III), whereas the reverse reaction was employed for the detection of Fe(III).

SVET experiments were performed using an instrument manufactured by Applicable Electronics Inc. (Forestdale, MA, USA). The sensing probe was a 10 µm PtIr tip with a black platinum deposit electrochemically grown to attain an adequate interfacial capacitance. Probe vibrations of 20 µm amplitude in both the normal and the parallel directions to the surface were applied, with 75 and 170 Hz respective vibration frequencies, maintaining a probe-substrate distance of 60 µm. Sample polarization was imposed using a potentiostat model 283 from EG&G Instruments (Princeton Applied Research, Oak Ridge, TN, USA). The analogic outputs for the current and the potential signals from the potentiostat were connected to the analogic inputs of the SVET instrument, in order to follow these signals during the experiments. An Ag/AgCl/KCl (3M) electrode was used as the reference. In order to minimize the occurrence of asymmetric current distributions in the solution adjacent to the steel surface that would produce eventual artefacts at the sensing probe, the counter electrode was a platinum ring covered with an electrodeposit of platinum black.

In selected experiments, a cathodic potential pulse was applied to the samples before recording the SVET measurements in order to modify the surface films formed on the samples. In those cases, the 283 potentiostat was controlled manually in order to apply to the sample the desired cathodic pulse during 6 seconds, followed by setting the desired anodic polarization during acquisition of the SVET scan. During all this procedure, the average currents flowing through the polarized sample was recorded by connecting the analogic output of the potentiostat to an A/D converter input available in the computer controlling the SVET instrument. Simultaneously, ionic current densities in the cell were measured as SVET signal with the probe located in a central location of the metal substrate.

3. Results and discussion

The effect of chloride concentration and pH on the susceptibility of 304 stainless steel was investigated using a combination of conventional and localized electrochemical methods with the aim to gain new insights concerning the distribution of electrochemical activity on the surface of the material, and its susceptibility to the onset of pitting corrosion. Spatially-resolved distributions of ionic currents and concentration gradients related to the formation of corrosion products were determined in the electrolyte phase containing chloride ions by using the scanning vibrating electrode technique (SVET) and scanning electrochemical microscopy (SECM). The metal samples were immersed in chloride-containing electrolytes of various compositions, namely 0.1 M NaCl, 0.1 M HCl, and 0.025 M HCl + 0.075 M $HClO_4$. The latter was chosen to contain a smaller concentration of chloride ions while maintaining the same pH than 0.1 M HCl solution, whereas 0.1 M NaCl and 0.1 M HCl solutions contained the same concentration of chloride ions.

3.1. Potentiodynamic polarization

The average susceptibility towards corrosion of 304 stainless steel was characterized by recording potentiodynamic polarization curves of the material in the three solutions under consideration. Typical anodic polarization curves are depicted in Figure 1, whereas Table 1 shows the main parameters related to the corrosion processes that were extracted from analysis of the curves. According to the OCP data, corrosion is favoured in the solutions containing the highest chloride concentration as expected, whereas a nobler surface was attained in the mixture of acids. A low pH does not seem to be as much an influential factor for this thermodynamic tendency as the chloride concentration, as indicated by the close OCP values determined in the hydrochloric acid and the sodium chloride solutions. Onset of passivity is observed in all the media, though the active – passive transition could not be discerned in either solution below the corresponding pitting potential. The lowest value for this E_{pit} was found in 0.1 M HCl. The related anodic current increase cannot occur in 0.1 M NaCl below 0.556 V vs. Ag/AgCl/KCl (3M), though current transients due to metastable pit formation are clearly distinguished. Conversely, in the 0.025 M HCl + 0.075 M $HClO_4$ medium, an abrupt increase in the current related to pitting corrosion was only observed when the sample was polarized at more anodic overpotentials, ca. +0.9 V vs. Ag/AgCl/KCl (3M).

Figure 1

Table 1

After the onset of pitting corrosion, 304 stainless steel could only repassivate in the less aggressive media consisting of the mixture of acids, as evidenced by the active passive transition found at +1.06 V vs. Ag/AgCl/KCl (3M), and the negative hysteresis observed when the potential sweep was reversed. In contrast, no repassivation was observed in the two solutions with higher chloride concentration, both exhibiting a positive hysteresis loop instead. This is also evidenced by the repassivation potential values, more positive in the HCl + $HClO_4$ containing environment, where repassivation occurs more easily. In all cases, E_{repas} values are more positive than the corresponding OCP, an indication of the high tendency of the 304 surface to spontaneously form a protective oxide layer, though the 0.1 M HCl medium requires smaller anodic polarizations for this to occur.

3.2. Scanning Vibrating Electrode Technique

Local effects related to polarization of the sample were evidenced by scanning the samples with the SVET. Current density distributions were first monitored over 304 stainless steel surfaces were exposed to 0.1 M HCl media whereas the samples were biased using a sequence of increasingly positive potential values. Only background noise was observed when the sample was either left unpolarized or polarized at 0 V vs. Ag/AgCl/KCl (3M). But substrate polarization at +0.10 V vs. Ag/AgCl/KCl (3M) showed the evolution of localized current density from a specific spot of the surface, as it can be seen in Figure 2A. Despite this low potential value, that is located within the passive region according to average data given in Table 1, the nucleated pit demonstrated to be stable because it was found at the same position in the following scans. They were recorded while applying progressively more positive polarizations to the substrate using 50 mV steps between subsequent scans. The SVET image recorded when the substrate was polarized at +0.30 V vs. Ag/AgCl/KCl (3M) is shown in Figure 2C, and the pit is already visible in the optical micrograph in Figure 2D that was recorded immediately before the scan was completed. It can be noticed that the anodic ionic currents originating from the pit grow with increasing positive polarization, as indicated by the scale bars provided in the figures. The SVET image also shows the initiation of a second stable pit that is located at the left of that previously described. Slightly negative current densities are seen during data acquisition in spite of the

anodic bias applied to the substrate, which should prevent any cathodic half reaction taking place over the steel substrate. This may arise from the technical limitations originating from asymmetries in the ionic currents flowing between the counter electrode and the substrate of different shapes. This lack of symmetry affects also the current distribution perpendicular to the substrate. These losses are interpreted by the equipment as cathodic currents after comparing the acquired data with the reference measurement taken just before each scan by placing the sensing probe above the centre of the substrate though separated ca. 3.5 mm above its surface.

Figure 2

A different behaviour was found by SVET when the steel sample was exposed to the sodium chloride solution. In agreement with the behaviour described by the polarization curve, no stable pitting corrosion could be detected with the SVET for the potentiostatically polarized specimen for potential values up to +0.40 V vs. Ag/AgCl/KCl (3M) (cf. Figure 3A). That is, the passive oxide film formed on the metal effectively protected it from the aggressive attack of the chloride ions in this natural pH solution. However, after the oxide film was effectively reduced by applying a polarization of -1.50 V vs. Ag/AgCl/KCl (3M) to the sample for approximately 3 seconds, in addition to hydrogen evolution as readily observed with the video camera, this treatment had a clear effect on the susceptibility of the sample towards corrosion. Indeed, new polarization of the sample at +0.40 V vs. Ag/AgCl/KCl (3M) revealed pit formation with the SVET, as shown in Figure 3B. In addition, there was a significant increase in the average current values measured with the potentiostat while scanning the surface. The same result was also obtained when recording a series of SVET images with increasing positive potential polarization applied to the sample, starting from -0.75 instead of 0 V vs. Ag/AgCl/KCl (3M), which led to the observation of pitting corrosion at lower positive potential values between +0.30 and +0.40 V vs. Ag/AgCl/KCl (3M) (not shown).

Figure 3

The observation of enhanced susceptibility towards corrosion after applying a negative potential to the specimen was further explored using conventional potentiodynamic polarization measurements. A freshly polished sample was immersed in

0.1 M NaCl solution, and subjected to potentiodynamic polarization starting at 0 V (which was the starting potential used for the substrate polarization in SVET measurements given in Figure 3), up to +0.50 V vs. Ag/AgCl/KCl (3M) (slightly below the E_{pit} value given in Table 1). At this potential, the direction of the potential sweep was reverted and the sample was polarized in the negative direction down to -1.50 V vs. Ag/AgCl/KCl (3M). Potential reversal was next applied and the potential was raised again up to +0.50 V vs. Ag/AgCl/KCl (3M), and finally swept in the negative direction down to +0.10 V vs. Ag/AgCl/KCl (3M). The corresponding current response during the application of this potential programme is shown in Figure 4. The initial anodic branch exhibits an anodic current plateau related to passive film formation without any sign of passivity breakdown. Upon potential reversal, the anodic current progressively decreases with smaller anodic overpotentials until the specimen attains cathodic polarization beyond the corresponding corrosion potential. During cathodic polarization, the current trace firstly depicts a plateau related to the diffusion-limited reduction of dissolved oxygen in the electrolyte, followed by the onset of the hydrogen evolution reaction (HER) at potentials more negative than -1.00 V vs. Ag/AgCl/KCl (3M). After potential reversal, the subsequent scan in the positive direction shows three main features. First, the open circuit potential was shifted to more negative potentials compared to that recorded for the passivated sample in the previous scan (namely -0.87 and -0.36 V vs. Ag/AgCl/KCl (3M), respectively). Secondly, the corrosion current extrapolated by graphical methods as the intersection of both Tafel slopes is in the order of 10^{-5} A cm^{-2} after the potential excursion down to -1.50 V vs. Ag/AgCl/KCl (3M), while that determined from the previous potential sweep in the same graph was one order of magnitude smaller. Finally, the anodic currents measured in the passive range around +0.45 V vs. Ag/AgCl/KCl (3M), denoted as (5) in the graph, are also one order of magnitude bigger than those recorded at the beginning of the experiment (marked as (1)), revealing the higher susceptibility of the material towards anodic dissolution after cathodic polarization. Furthermore, a hysteresis loop was also observed following the last potential reversal produced at +0.50 V vs. Ag/AgCl/KCl (3M), indicating some breakdown of the passive layer formed in these conditions. It is thought that these observations support the previous findings from SVET measurements.

Figure 4

The effect of electrochemical reduction of the oxide layer was further investigated using SVET while subjecting the sample to a two-step polarization programme. It consisted in the application of a cathodic potential relative to the OCP for 5 seconds, followed by anodic polarization of the sample at +0.45 V vs. Ag/AgCl/KCl (3M) during one minute. We recorded both the average current flowing through the sample, monitored at the output of the potentiostat, and the current density registered with the SVET probe placed above the centre of the metal strip. Figure 5 gives the temporal evolution of these current signals during anodic polarization of the sample, immediately following previous application of a cathodic polarization at various potential values. Short cathodic potential pulses at -1.00 V vs. Ag/AgCl/KCl (3M), effectively increased the susceptibility of the steel sample towards metal dissolution during anodic polarization for the given time and potential. This is evidenced in Figure 5A through the increasing average currents that are measured from the sample. When a more negative potential value was applied during the cathodic pulse, namely -1.10 V vs. Ag/AgCl/KCl (3M), the subsequent anodic current transient exhibited a continuous increase in the current related to the propagation of a localized corrosion process at the metal surface. Variations in the ionic current flows measured at the SVET probe with time occurred almost at the same times that those reported in the average current (cf. Figure 5B). In this case, negative ionic current densities were recorded during the prior application of the cathodic step, with greater absolute values the more negative potential applied. This cathodic potential was maintained during 6 seconds in all cases, therefore the SVET signals are related to the flux of anions generated through the cathodic processes taking place on the surface. Next, the application of less negative values to the substrate prior to the anodic pulse led to the measurement of positive ionic current flows almost two orders of magnitude greater during the subsequent application of the anodic polarization. The anodic current flows are due to diffusion of the iron cations generated at the surface, thus supporting that enhanced metal dissolution occurred in the system, as it is expected in the case of a localized corrosion process. Finally, the signals determined with the SVET probe dropped to those typically corresponding to background noise levels upon ceasing substrate polarization (for times longer than 66 s), an indication of substrate repassivation.

Figure 5

A different behaviour was observed in the 25 mM HCl + 75 mM $HClO_4$. No localized electrochemical activity was observed with the SVET + potentiostat combination for anodic polarization of the substrate up to +0.45 V vs. Ag/AgCl/KCl (3M) following cathodic pulses in the -0.80 to -2.00 V vs. Ag/AgCl/KCl (3M) range. This indicates that passive layer breakdown is promoted by the action of chloride ions rather than pH. However, electrolyte exchange between 0.1 M NaCl and 25 mM HCl + 75 mM $HClO_4$ solutions led to pitting corrosion on the steel surface. This was done as it follows: initially, the substrate was immersed in the hydrochoric – perchloric acid solution and polarized anodically (without prior application of a cathodic potential to the cell). Subsequently, electrolyte exchange using conductivity water followed by addition of 0.1 M NaCl solution was performed, whereas the substrate was left at its spontaneous open circuit potential during this stage of the procedure, and SVET images were collected as before. Next, the electrolyte was exchanged to the mixed acid solution in order to repeat the anodic polarization step though with the substrate polarized at a more positive potential value than in the preceding step. New exchange of electrolyte solution to 0.1 M NaCl will be subsequently performed to record the corresponding SVET image. Active pitting corrosion in 0.1 M NaCl solution of the unpolarised sample occurred following the anodic polarization at +0.35 V vs. Ag/AgCl/KCl (3M) in the acid solution (see Figure 6). This local activation of the surface was better observed following polarization at +0.40 V vs. Ag/AgCl/KCl (3M).

Figure 6

3.3. Scanning Electrochemical Microscopy

SECM measurements carried out with substrate immersed in 0.1 M HCl were done by recording scan lines along the X axis at different fixed Y positions. Increasing polarizations were applied to the steel substrate, starting from the OCP and finishing with +0.40 V vs. Ag/AgCl/KCl (3M) anodic polarization. Figure 7 displays various selections of scan lines chosen to describe the trends observed during the measurements under different polarization conditions. The experiment was initiated by recording scan lines over the unpolarized sample. The tip potential was set at +0.50 V vs. Ag/AgCl/KCl (3M) to follow the oxidation of the iron (II) species evolving from the surface due to metal dissolution. Then, metal dissolution will be detected by measuring faradaic currents at the SECM tip when it

passes above the active corroding site. This was indeed the case especially along the first scan lines recorded in the series, those exhibiting the smallest *Y* coordinates in Figure 7A. A tip current peak reaching ca. 100 pA is present in the first scan line, and it progressively became less notorious towards the end of the experimental series, that is, in those lines recorded with the tip scanning with the biggest *Y* coordinates.

Figure 7

Subsequently, the experimental sequence was repeated for various polarizations of the substrate extending from 0 V to more positive values using 100 mV steps. No metal dissolution was detected for the scan lines recorded at 0, +0.10 and +0.20 V vs. Ag/AgCl/KCl (3M) (not shown in the Figure). The values of the tip currents recorded in the scan lines could not be separated from the background noise level. Unambiguous current values were recorded when the substrate was polarized at +0.30 V vs. Ag/AgCl/KCl (3M), though they amounted only a few pA (see Figure 7B). Since the potential applied to the substrate was positive enough from a thermodynamic standpoint to oxidize the iron (II) species formed as result of the anodic dissolution of the substrate, the surface was scanned over the same scan line exhibiting that signal while setting the tip to +0.10 V vs. Ag/AgCl/KCl (3M). In this way, eventual formation of iron (III) species at that active site on the surface would be detected on the subsequent current trace drawn in red in Figure 7B. It is readily observable that currents related to iron reduction were not detected from the system. This fact may support that the corroding 304 stainless steel substrate does not produce iron (III) species, neither it provides a surface for electron transfer that would produce the oxidation of the dissolving ferrous ions in this acid environment.

Polarization of the substrate at +0.40 V vs. Ag/AgCl/KCl (3M) was accompanied by the recording of greater currents at the tip associated with iron (II) collection, as observed in Figure 7C. This observation is consistent with the greater anodic currents observed at this potential in the potentiodynamic polarization curve of 304 steel in 0.1 M HCl shown in Figure 1. Oxidation of iron (II) ions occurred exclusively at the tip despite the high positive polarization applied to the substrate. This feature is supported by the measurement of zero tip currents related to iron (III) reduction in the scan lines recorded when the tip potential was set at +0.10 V vs. Ag/AgCl/KCl (3M). Furthermore, no evidence for the anodic dissolution of the steel with the formation of iron (III) species could be found. Besides, with such corrosion rate, substrate current in this experiment surprisingly seemed to be

influenced by the tip location. As observed in Figure 7D, which shows current of the substrate recorded while measuring lines given in Figure 7C, when tip was passing across the metal target, located in the centred position, current detected at the sample significantly decreased when probe was biased at either +0.10 or +0.50 V vs. Ag/AgCl/KCl (3M). In order to give an explanation to this phenomenon we must first consider that the microelectrode is effectively altering the electrochemical properties of the local media in the close proximity of the sample. Then, tip polarization at +0.50 V vs. Ag/AgCl/KCl (3M) and subsequent oxidation of iron to the ferric form could lead to a temporary passive layer formation, since iron (III) is more likely to form hydroxides. However, at this low pH, the hydroxide formation is not so spontaneous, though cannot be discarded at this highly localized range and further exploration of the surrounding media must be given to clarify this. On the other hand, when tip is biased at +0.10 V vs. Ag/AgCl/KCl (3M), apparently there is no electrochemical process taking place at the tip since no current is detected, so the mentioned alteration of the electrochemical properties of the local media does not seem to be enough to explain that effect. Then, the reason might simply arise from the convection produced by the tip movement, which refresh the solution, probably more acidified during the anodic substrate polarization (and consequently more aggressive) due to the partial hydrolysis of iron cations.

A similar procedure was not performed in the low-containing chloride solution 25 mM HCl + 75 mM $HClO_4$ since it did not show any significant activity related to passivity breakdown by SVET.

On the contrary, SECM characterization of 304 stainless steel in 0.1 M NaCl solution was conducted for the sample subjected to stable pitting conditions. Upon immersion of the freshly polished samples in the test solution, cathodic pulses were applied in order to promote pitting corrosion during subsequent polarization at +0.45 V vs. Ag/AgCl/KCl (3M). Then, SECM measurements were carried with the tip sequentially polarized at +0.10 and +0.50 V vs. Ag/AgCl/KCl (3M), while the substrate was held at +0.45 V vs. Ag/AgCl/KCl (3M). Figure 8 shows the SECM maps recorded with the tip polarized at both potentials. 2D scans were recorded instead of scan lines because the media was less aggressive, and it was harder to locate the precise location at which surface activation would occur. Data collected for E_{tip} = +0.50 V vs. Ag/AgCl/KCl (3M) are mostly small current values which are even smaller at the centre of the scanned area, where the steel substrate was placed. This behaviour is accompanied by the observation that this surface was showing dissolution currents in the order of hundreds of microamperes. Thus, there is less iron (II) available for

oxidation into iron (III) at the tip in the proximity of the sample, providing a response similar to that observed for competitive behaviour. This can be explained considering that in this media the surface is now able to oxidize the iron (II) species from metal dissolution, and iron (III) is the main species formed under these conditions. Furthermore, ferrous ions are produced in a smaller amount, and they can be oxidized on the active metallic sample before diffusing into the electrolyte. This oxidation reaction on the corroding surface of steel is more easily attained in near neutral conditions due to the higher tendency of iron (III) to form hydroxides, a reaction that shifts the equilibrium of iron oxidation to the ferric ion formation. This feature is also evidenced by the negative currents detected from specific locations in a central position of the map recorded for E_{tip} = +0.10 V vs. Ag/AgCl/KCl (3M) that is given in Figure 8B. These rather high cathodic current values arise from active sites where ferric ions are being produced. However, it is also observed a significant increase of the anodic current at the end of the lines of the scans, precisely where those cathodic intensities were detected.

Figure 8

Substrate current was then also monitored during scan acquisition. Major variations could be observed during the 3 hours required to record the two SECM images in Figure 8. A selection of the current response measured at the substrate is given in Figure 9. Most of them, especially those corresponding to linear scans taken while the tip acquired the lines corresponding to *Y* positions close the half of duration, showed current depletion effects with the proximity of the tip, as it was previously observed in HCl solution. Then, pH background is not (at least not the only one) key factor responsible for this phenomenon, but local pH changes, tip convection and local modification of the electrochemical media should also be considered. Thus, the justification given above will also account for this observation.

Figure 9

4. Conclusions

The effect that substrate polarization in 304 stainless steel surfaces produces on the anodic dissolution of the metallic material has been explored. SVET and SECM results indicate vigorous anodic local dissolution in 0.1 M HCl solution, while prior removal or weakening of the passive layer is mandatory to obtain comparable results in 0.1 M NaCl solution. The controlled modification of acidity and chloride ion concentration in the aqueous solution facilitated the onset of anodic local dissolution to be observed by SVET.

SECM experiments have led to identification of the ionic iron species formed during metal dissolution and their distribution above the exposed sample. Release of iron (II) ions was mostly observed in 0.1 HCl media, but major production of iron (III) was detected in 0.1 M NaCl media when the pitting range was reached for 304 surfaces.

Acknowledgments

This work was financially supported by the Spanish Ministry of Economy and Competitiveness (MINECO, Madrid, Spain) jointly with the European Regional Development Fund (Brussels, Belgium) under grant CTQ2012-36787. The award of a Research Training Grant to J.I. by the Spanish Ministry of Education (*Programa de Formación de Personal Investigador*, Madrid, Spain) is greatly appreciated.

References

1. M.V. Biezma, J.R. San Cristóbal, Methodology to study cost of corrosion, Corrosion Engineering Science and Technology 40 (2005) 344-352.
2. C.-O.A. Olsson, D. Landolt, Film growth during anodic polarization in the passive region on 304 stainless steels with Cr, Mo, or W additions studied with EQCM and XPS, Journal of the Electrochemical Society 148 (2001) B438-B449.
3. D. Hamm, C.-O.A. Olsson, D. Landolt, Effect of chromium content and sweep rate on passive film growth on iron–chromium alloys studied by EQCM and XPS, Corrosion Science 44 (2002) 1009-1025.
4. K.-T. Oh, K.-N. Kim, M. Lee, Y.-S. Park, Corrosion wear of high molybdenum and nitrogen stainless steel for biomedical applications, Journal of the Electrochemical Society 149 (2002) B146-B153.

5. E.-S.M. Sherif, J.H. Potgieter, J.D. Comins, L. Cornish, P.A. Olubambi, C.N. Machio, The beneficial effect of ruthenium additions on the passivation of duplex stainless steel corrosion in sodium chloride solutions, Corrosion Science 51 (2009) 1364-1371.
6. E.-S.M. Sherif, J.H. Potgieter, J.D. Comins, L. Cornish, P.A. Olubambi, C.N. Machio, Effects of minor additions of ruthenium on the passivation of duplex stainless-steel corrosion in concentrated hydrochloric acid solutions, Journal of Applied Electrochemistry 39 (2009) 1385-1392.
7. Y. Jiang, H. Tan, Z. Wang, J. Hong, L. Jiang, J. Li, Influence of Cr_{eq}/Ni_{eq} on pitting corrosion resistance and mechanical properties of UNS S32304 duplex stainless steel welded joints, Corrosion Science 70 (2013) 252-259.
8. A. Legat, V. Doleček, Chaotic analysis of electrochemical noise measured on stainless steel, Journal of the Electrochemical Society 142 (1995) 1851-1858.
9. F.J. Pérez, M.P. Hierro, C. Gómez, L. Martínez, P.G. Viguri, Ion implantation as a surface modification technique to improve localised corrosion of different stainless steels, Surface and Coatings Technology 155 (2002) 250-259.
10. C.X. Li, T. Bell, Corrosion properties of active screen plasma nitrided 316 austenitic stainless steel, Corrosion Science 46 (2004) 1527-1547.
11. C.X. Li, T. Bell, Corrosion properties of plasma nitrided AISI 410 martensitic stainless steel in 3.5% NaCl and 1% HCl aqueous solutions, Corrosion Science 48 (2006) 2036-2049.
12. G.H. Aydoğdu, M.K. Aydinol, Determination of susceptibility to intergranular corrosion and electrochemical reactivation behaviour of AISI 316L type stainless steel, Corrosion Science 48 (2006) 3565-3583.
13. K. Prabakaran, S. Rajeswari, Electrochemical, SEM and XPS investigations on phosphoric acid treated surgical grade type 316L SS for biomedical applications, Journal of Applied Electrochemistry 39 (2009) 887-897.
14. M. Azzi, M. Benkahoul, J.E. Klemberg-Sapieha, L. Martinu, Corrosion and mechanical properties of duplex-treated 301 stainless steel, Surface and Coatings Technology 205 (2010) 1557-1563.
15. E.A. Ferreira, R.D. Noce, C.S. Fugivara, A.V. Benedetti, Evaluation of 316L stainless steel corrosion resistance in solution simulating the acid hydrolysis of biomass, Journal of the Electrochemical Society 158 (2011) C95-C103.
16. E. Heitz, DC electrochemical methods, in: Analytical Methods in Corrosion Science and Engineering (P. Marcus, F. Mansfeld, Eds.); CRC Press, Boca Raton, FL (2006), p. 435-462.

17. F. Huet, Electrochemical noise technique, in: Analytical Methods in Corrosion Science and Engineering (P. Marcus, F. Mansfeld, Eds.); CRC Press, Boca Raton, FL (2006), p. 507-570.
18. F. Mansfeld, Electrochemical impedance spectroscopy, in: Analytical Methods in Corrosion Science and Engineering (P. Marcus, F. Mansfeld, Eds.); CRC Press, Boca Raton, FL (2006), p. 463-505.
19. H. Böhni, T. Suter, F. Assi, Micro-electrochemical techniques for studies of localized processes on metal surfaces in the nanometer range, Surface and Coatings Technology 130 (2000) 80-86.
20. T. Suter, H. Böhni, The microcell technique, in: Analytical Methods in Corrosion Science and Engineering (P. Marcus, F. Mansfeld, Eds.); CRC Press, Boca Raton, FL (2006), p. 649-696.
21. F. Arjmand, A. Adriaens, Investigation of 304L stainless steel in a NaCl solution using a microcapillary electrochemical droplet cell: Comparison with conventional electrochemical techniques, Electrochimica Acta 59 (2012) 222-227.
22. J. Li, D.J. Meier, An AFM study of the properties of passive films on iron surfaces, Journal of Electroanalytical Chemistry 454 (1998) 53-58.
23. V. Maurice, P. Marcus, Scanning tunneling microscopy and atomic force microscopy, in: Analytical Methods in Corrosion Science and Engineering (P. Marcus, F. Mansfeld, Eds.); CRC Press, Boca Raton, FL (2006), p. 133-168.
24. L. Liu, Y. Li, F. Wang, Pitting mechanism on an austenite stainless steel nanocrystalline coating investigated by electrochemical noise and *in-situ* AFM analysis, Electrochimica Acta 54 (2008) 768-780.
25. L. Niu, Y. Yin, W. Guo, M. Lu, R. Qin, S. Chen, Application of scanning electrochemical microscope in the study of corrosion of metals, Journal of Materials Science, 44 (2009) 4511-4521.
26. M.B. Jensen, D.E. Tallman, Application of SECM to corrosion studies, in: Electroanalytical Chemistry: A Series of Advances, vol. 24 (A.J. Bard, C.G. Zoski, Eds.); CRC Press, Boca Raton (2012), p. 171-286.
27. T. Misawa, H. Tanabe, In-situ observation of dynamic reacting species at pit precursors of nitrogen-bearing austenitic stainless steels, ISIJ International 36 (1996) 787-792.
28. J. Izquierdo, L. Nagy, J.J. Santana, G. Nagy, R.M. Souto, A novel microelectrochemical strategy for the study of corrosion inhibitors employing the scanning vibrating electrode technique and dual potentiometric/amperometric operation in scanning

electrochemical microscopy: Application to the study of the cathodic inhibition by benzotriazole of the galvanic corrosion of copper coupled to iron, Electrochimica Acta 58 (2011) 707-716.

29. J. Izquierdo, L. Nagy, Á. Varga, J.J. Santana, G. Nagy, R.M. Souto, Spatially resolved measurement of electrochemical activity and pH distributions in corrosion processes by scanning electrochemical microscopy using antimony microelectrode tips, Electrochimica Acta 56 (2011) 8846-8850.
30. J. Izquierdo, L. Nagy, S. González, J.J. Santana, G. Nagy, R.M. Souto, Resolution of the apparent experimental discrepancies observed between SVET and SECM for the characterization of galvanic corrosion reactions, Electrochemistry Communications 27 (2013) 50-53.
31. R.M. Souto, Y. González-García, S. González, In situ monitoring of electroactive species by using the scanning electrochemical microscope. Application to the investigation of degradation processes at defective coated metals, Corrosion Science 47 (2005) 3312-3323.
32. E. Völker, C. González-Inchauspe, E.J. Calvo, Scanning electrochemical microscopy measurement of ferrous ion fluxes during localized corrosion of steel, Electrochemistry Communications 8 (2006) 179-183.
33. A.M. Simões, A.C. Bastos, M.G. Ferreira, Y. González-García, S. González, R.M. Souto, Use of SVET and SECM to study the galvanic corrosion of an iron–zinc cell, Corrosion Science 49 (2007) 726-739.
34. Y. Yin, L. Niu, M. Lu, W. Guo, S. Chen, In situ characterization of localized corrosion of stainless steel by scanning electrochemical microscope, Applied Surface Science 255 (2009) 9193-9199.
35. M. Terada, A. F. Padilha, A. M. P. Simões, H. G. de Melo, I. Costa, Use of SECM to study the electrochemical behavior of DIN 1.4575 superferritic stainless steel aged at 475 ºC, Materials and Corrosion 60 (2009) 889-894.
36. Y. Yuan, L. Li, C. Wang, Y. Zhu, Study of the effects of hydrogen on the pitting processes of X70 carbon steel with SECM, Electrochemistry Communications 12 (2010) 1804-1807.
37. R.M. Souto, J.J. Santana, L. Fernández-Mérida, S. González, Sensing electrochemical activity in polymer coated metals during the early stages of coating degradation – Effect of the polarization of the substrate, Electrochimica Acta 56 (2011) 9596-9601.
38. M. Terada, R.A. Marques, A.M. Simões, A.F. Padilha, I. Costa, Use of SECM to compare corrosion resistance of DIN W. Nr. 1.4460 high N and AISI 316L austenitic stainless steels in

physiological solutions, Corrosion Engineering Science and Technology 46 (2011) 599-604.

39. A. Pilbáth, T. Szabó, J. Telegdi, L. Nyikos, SECM study of steel corrosion under scratched microencapsulated epoxy resin, Progress in Organic Coatings 75 (2012) 480-485.
40. K. Fushimi, K.A. Lill, H. Habazaki, Heterogeneous hydrogen evolution on corroding Fe–3 at.% Si surface observed by scanning electrochemical microscopy, Electrochimica Acta 52 (2007) 4246-4253.
41. J.J. Santana, J. González-Guzmán, L. Fernández-Mérida, S. González, R.M. Souto, Visualization of local degradation processes in coated metals by means of scanning electrochemical microscopy in the redox competition mode, Electrochimica Acta 55 (2010) 4488-4494.
42. R. Leiva-García, R. Akid, D. Greenfield, J. Gittens, M.J. Muñoz-Portero, J. García-Antón, Study of the sensitisation of a highly alloyed austenitic stainless steel, Alloy 926 (UNS N08926), by means of scanning electrochemical microscopy, Electrochimica Acta 70 (2012) 105-111.
43. J.A. Wharton, B.G. Mellor, R.J.K. Wood, C.J.E. Smith, Crevice corrosion studies using electrochemical noise measurements and a scanning electrode technique, Journal of the Electrochemical Society 147 (2000) 3294-3301.
44. H. Uchida, M. Yamashita, S. Inoue, K. Koterazawa, In-situ observations of crack nucleation and growth during stress corrosion by scanning vibrating electrode technique, Materials Science and Engineering A 319-321 (2001) 496-500.
45. B. Vuillemin, X. Philippe, R. Oltra, V. Vignal, L. Coudreuse, L.C. Dufour, E. Finot, SVET, AFM and AES study of pitting corrosion initiated on MnS inclusions by microinjection, Corrosion Science 45 (2003) 1143-1159.
46. H. Krawiec, V. Vignal, R. Oltra, Use of the electrochemical microcell technique and the SVET for monitoring pitting corrosion at MnS inclusions, Electrochemistry Communications 6 (2004) 655-660.
47. H.E. Jamil, A. Shriri, R. Boulif, C. Bastos, M.F. Montemor, M.G.S. Ferreira, Electrochemical behaviour of amino alcohol-based inhibitors used to control corrosion of reinforcing steel, Electrochimica Acta 49 (2004) 2753-2760.
48. A.C. Bastos, M.G. Ferreira, A.M. Simões, Corrosion inhibition by chromate and phosphate extracts for iron substrates studied by EIS and SVET, Corrosion Science 48 (2006) 1500-1512.

49. H. Iken, R. Basseguy, A. Guenbour, A. Ben Bachir, Classic and local analysis of corrosion behaviour of graphite and stainless steels in polluted phosphoric acid, Electrochimica Acta 52 (2007) 2580-2587.
50. V. Vignal, H. Krawiec, O. Heintz, R. Oltra, The use of local electrochemical probes and surface analysis methods to study the electrochemical behaviour and pitting corrosion of stainless steels, Electrochimica Acta 52 (2007) 4994-5001.
51. M. Reffass, R. Sabot, M. Jeannin, C. Berziou, Ph. Refait, Effects of NO_2^- ions on localised corrosion of steel in $NaHCO_3$ + NaCl electrolytes, Electrochimica Acta 52 (2007) 7599-7606.
52. M. Reffass, R. Sabot, M. Jeannin, C. Berziou, Ph. Refait, Effects of phosphate species on localised corrosion of steel in $NaHCO_3$ + NaCl electrolytes, Electrochimica Acta 54 (2009) 4389-4396.
53. A. Alvarez-Pampliega, M.G. Taryba, K. Van den Bergh, J. De Strycker, S.V. Lamaka, H. Terryn, Study of local Na^+ and Cl^- distributions during the cut-edge corrosion of aluminum rich metal-coated steel by scanning vibrating electrode and micro-potentiometric techniques, Electrochimica Acta 102 (2013) 319-327.
54. G.A. Zhang, Y.F. Cheng, Corrosion of X65 steel in CO_2-saturated oilfield formation water in the absence and presence of acetic acid, Corrosion Science 51 (2009) 1589-1595.

Table 1. Average parameters obtained from the potentiodynamic polarization curves of 304 stainless steel. All potential values are referred to the Ag/AgCl/KCl (3M) reference electrode.

	0.1 M NaCl	0.025 M HCl + 0.075 M $HClO_4$	0.1 M HCl
E_{OCP}, V	-0.203	0.159	-0.176
E_{pass}, V	-	0.239	-
E_{pit}, V	0.556	0.907	0.148
E_{repas}, V	-0.129	0.547	-0.093
j_{corr}, µA cm^{-2}	1.36	1.05	0.753
j_{pass}, µAcm^{-2}	-	10.4	-

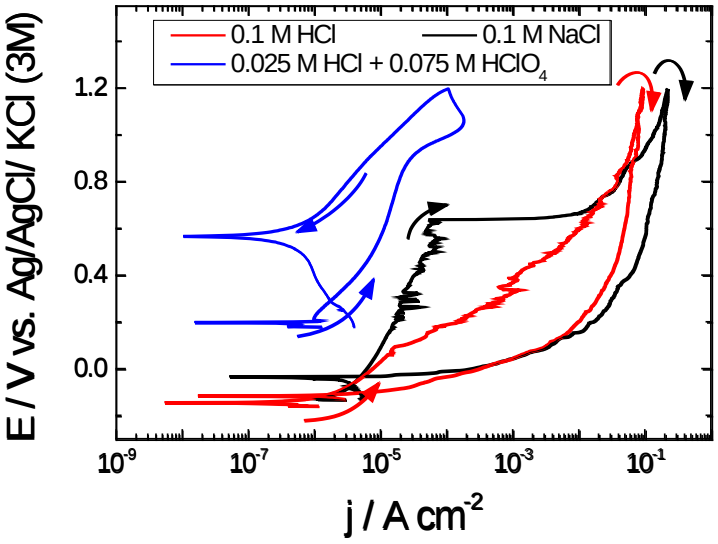

Figure 1. Typical potentiodynamic polarization curves of 304 stainless steel samples immersed in the solutions indicated in the plot. Scan rate: 1 mV s^{-1}.

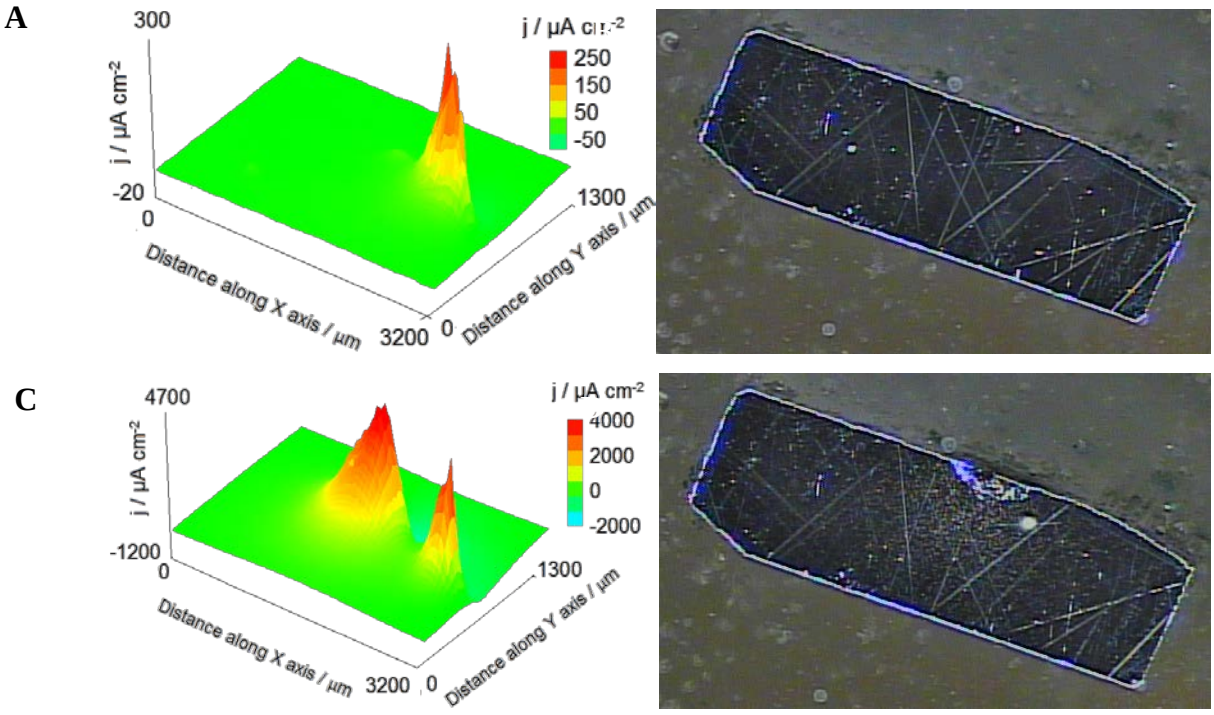

Figure 2. SVET images (A,C) and optical micrographs (B,D) of 304 stainless steel surface immersed in 0.1 M HCl. Polarization values applied to the substrate: (A,B) +0.10, and (C,D) +0.30 V vs. Ag/AgCl/KCl (3M).

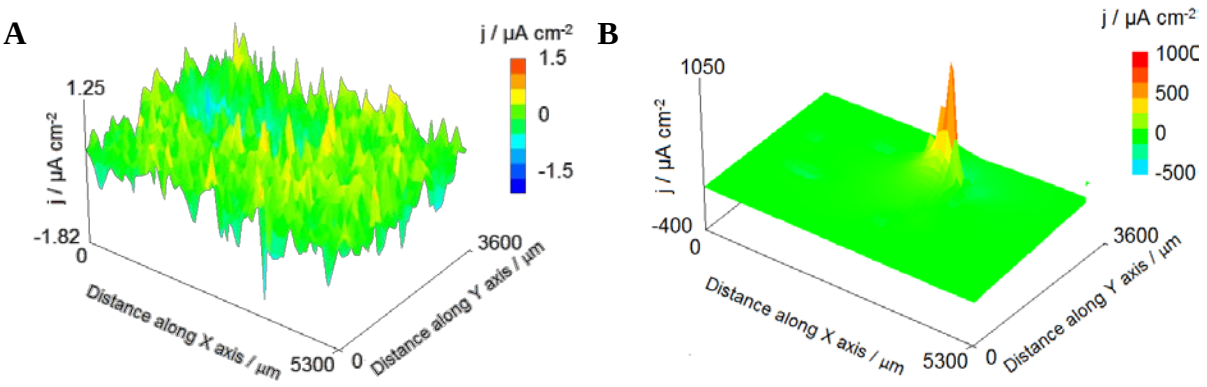

Figure 3. SVET images of a 304 stainless steel sample polarized at +0.40 V vs. Ag/AgCl/KCl (3M) during immersion in 0.1 M NaCl. They were recorded before (A) and after (B) the application to the sample of a cathodic potential pulse at -1.50 V vs. Ag/AgCl/KCl (3M) during 3 s.

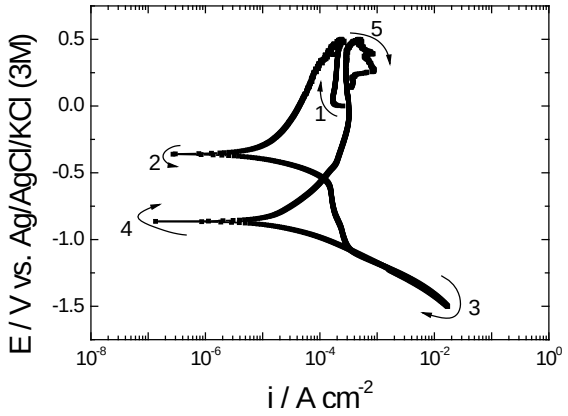

Figure 4. Potentiodynamic polarization of a 304 stainless steel sample in 0.1 M NaCl. Numbers and arrows in the graph indicate the sequence and the direction of the polarization sweeps applied to the sample. Scan rate: 1 mV s^{-1}.

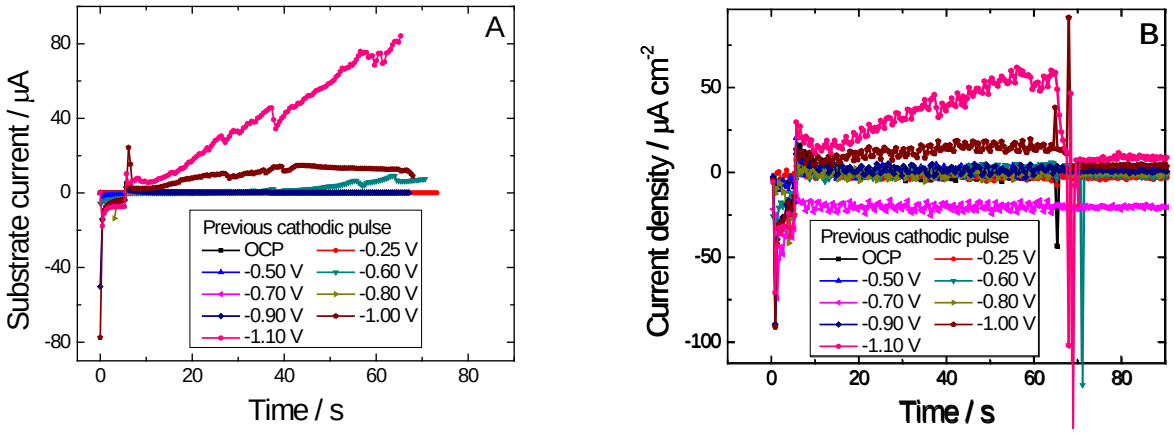

Figure 5. Time evolution of the average and local currents flowing during the immersion of a 304 stainless steel sample immersed in 0.1 M NaCl. The sample was polarized at +0.45 V vs. Ag/AgCl/KCl (3M) following the application of a cathodic pulse during 5 seconds. The values of the cathodic polarizations are indicated in the plots referred to the Ag/AgCl/KCl (3M) reference electrode. (A) Total current flowing through the specimen, and (B) local ionic current densities detected at the SVET probe placed over the centre of the metal strip.

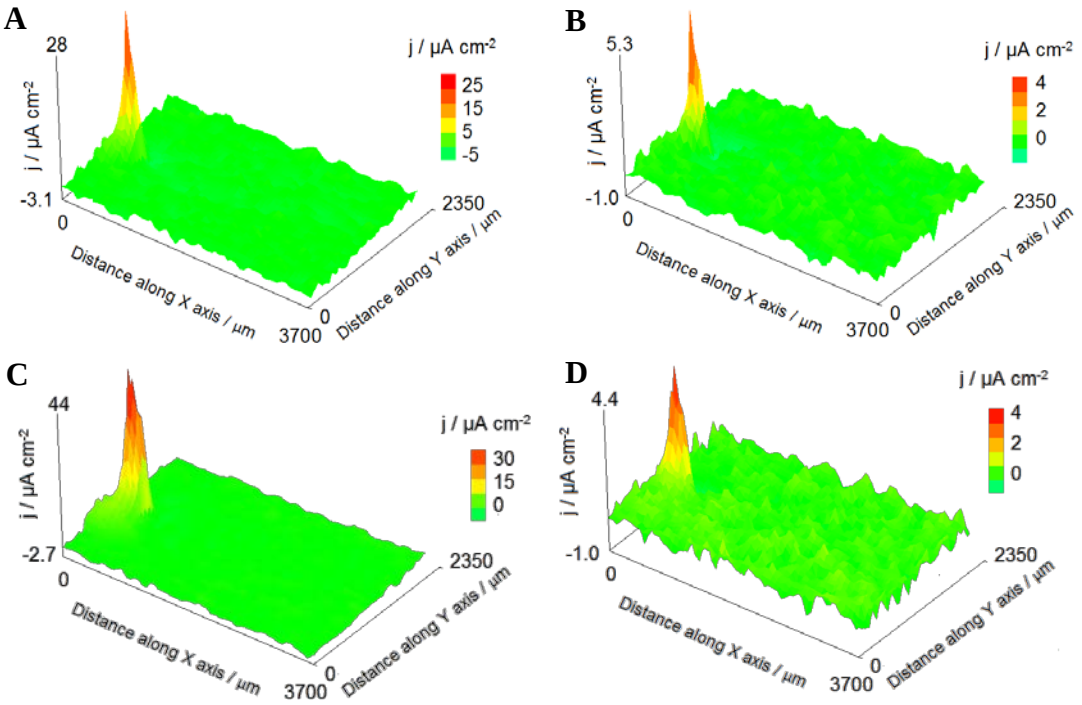

Figure 6. SVET images of a 304 stainless steel sample recorded during immersion in (A,C) 25 mM HCl + 75 mM $HClO_4$, or in (B,D) 0.1 M NaCl following solution exchange. Polarization conditioning of the sample: (A) polarized at +0.35 V vs. Ag/AgCl/KCl (3M), (B,D) open circuit potential, and (C) polarized at +0.40 V vs. Ag/AgCl/KCl (3M).

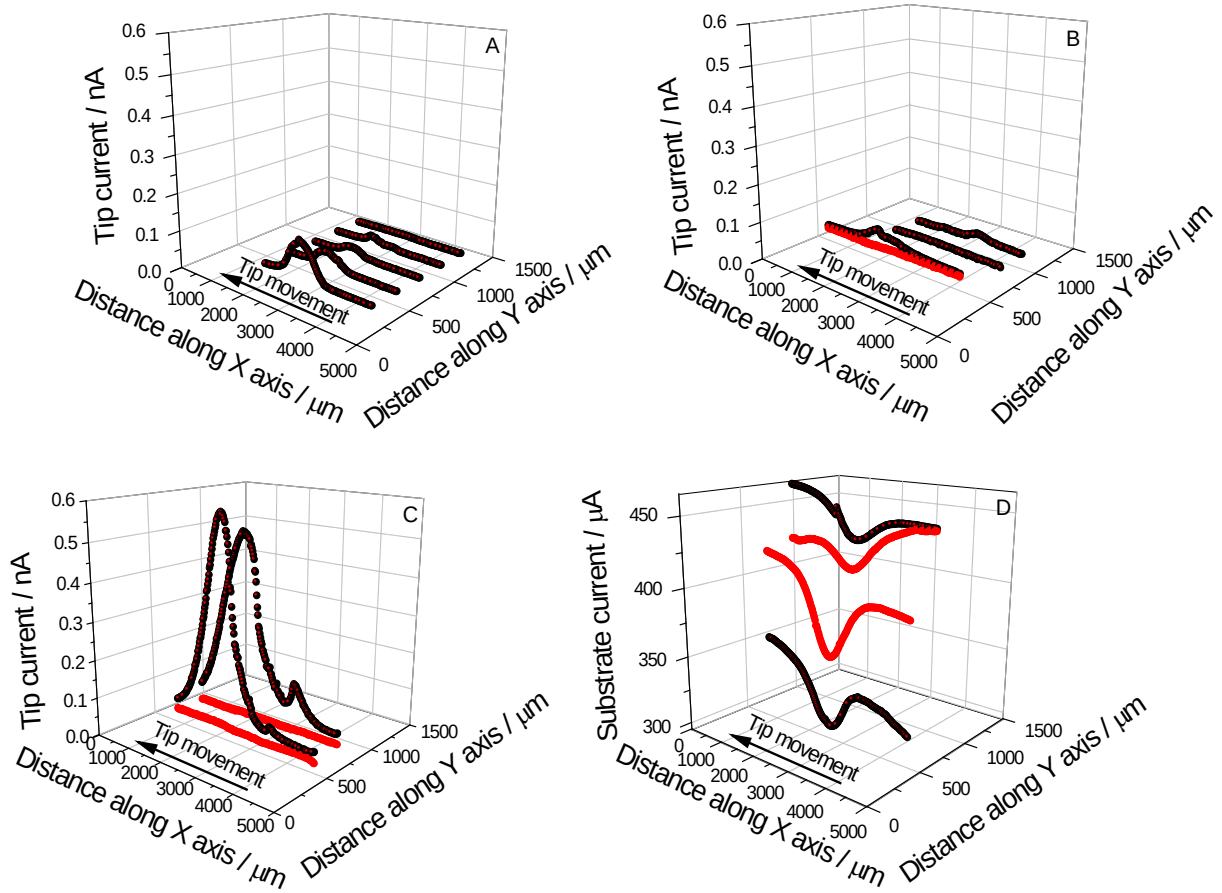

Figure 7. Current recorded either at the ultramicroelectrode (A,B,C) or at the 304 stainless steel substrate (D) during immersion in 0.1 M HCl solution. Potential condition at the substrate: (A) OCP, (B) +0.30, and (C, D) +0.40 V vs. Ag/AgCl/KCl (3M). Current recordings were performed while the tip was scanned across the steel strip using: tip-substrate distance: 10 µm; scan rate: 25 µm s^{-1}. Tip potential: (black) +0.50 V vs. Ag/AgCl/KCl (3M) for the oxidation of Fe(II) species; (red) +0.10 V vs. Ag/AgCl/KCl (3M) for the reduction of Fe(III) species.

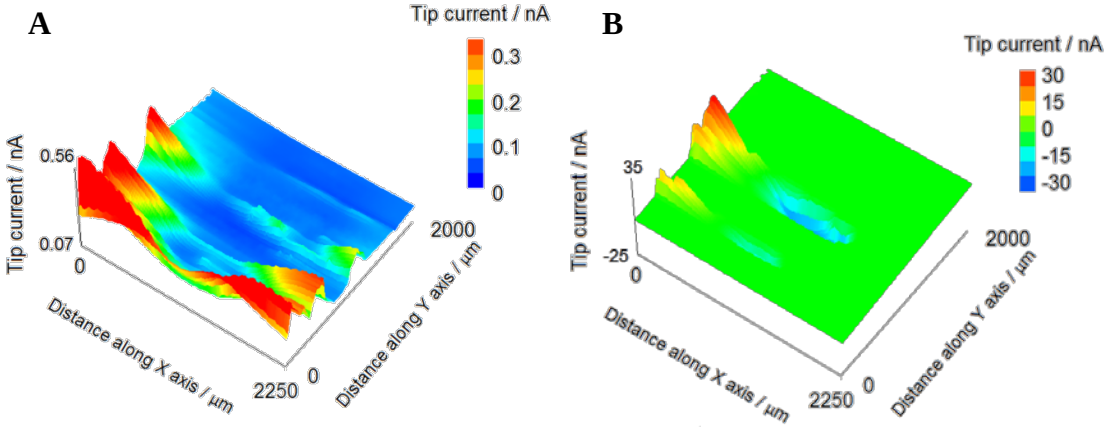

Figure 8. SECM maps recorded over the 304 stainless steel substrate biased at +0.45 V vs. Ag/AgCl/KCl (3M) during immersion in 0.1 M HCl. Substrate polarization is located inside the pitting regime of the material. Tip potential: (A) +0.50, and (B) +0.10 V vs. Ag/AgCl/KCl (3M); tip-substrate distance: 10 µm; scan rate: 25 µm s^{-1}.

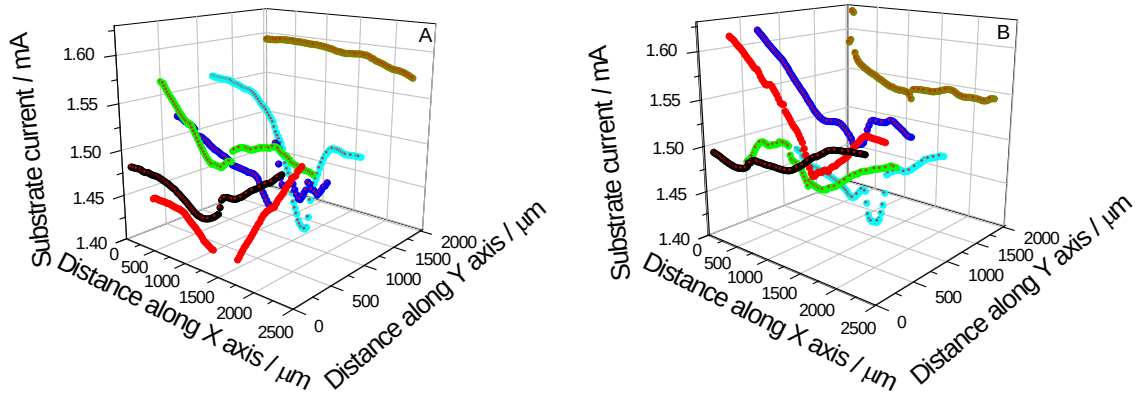

Figure 9. Current recorded at the 304 stainless steel surface immersed in 0.1 M NaCl while recording the SECM maps shown in Figure 8. E_{tip}: (A) +0.50, and (B) +0.10 V vs. Ag/AgCl/KCl (3M).